

Article

Structural, Non-Covalent Interaction, and Natural Bond Orbital Studies on Bromido-Tricarbonyl Rhenium(I) Complexes Bearing Alkyl-Substituted 1,4-Diazabutadiene (DAB) Ligands

Reza Kia * and Azadeh Kalaghchi

Chemistry Department, Sharif University of Technology, Tehran P.O. Box 11155-3516, Iran; azade_ka8757@yahoo.com

* Correspondence: rkia@sharif.edu or zsrkk@yahoo.com; Tel.: +98-21-66165332; Fax: +98-21-66029165

Received: 28 February 2020; Accepted: 31 March 2020; Published: 1 April 2020



Abstract: The synthesis, characterization, structural and computational studies of Re(I) tricarbonyl bromo complexes bearing alkyl-substituted 1,4-diazabutadiene ligands, $[\text{Re}(\text{CO})_3(1,4\text{-DAB})\text{Br}]$, where 1,4-DAB = *N,N*-bis(2,4-dimethylbenzene)-1,4-diazabutadiene, $^{2,4}\text{Me}_2\text{DAB}$ (**1**); *N,N*-bis(2,4-dimethylbenzene)-2,3-dimethyl-1,4-diazabutadiene, $^{2,4}\text{Me}_2\text{DAB}^{\text{Me}}$ (**2**); *N,N*-bis(2,4,6-trimethylbenzene)-1,4-diazabutadiene, $^{2,4,6}\text{Me}_3\text{DAB}$ (**3**); and *N,N*-bis(2,6-diisopropylbenzene)-1,4-diazabutadiene, $^{2,6}\text{-ipr}_2\text{DAB}$ (**4**) are reported. The complexes were characterized by different spectroscopic methods such as FT-IR, $^1\text{H-NMR}$, $^{13}\text{C-NMR}$, and elemental analyses and their solid-state structures were confirmed by X-ray diffraction. In each complex, the Re(I) centre shows a distorted octahedral shape with a facial geometry of carbonyl groups. The gas phase geometry of the complexes was identified by density functional theory. Interesting intermolecular $n \cdots \pi^*$ interactions of complexes **1** and **3** were investigated by non-covalent interaction index (NCI), and natural bond orbital (NBO) analyses. The intramolecular $n \cdots \sigma^*$, $\sigma \cdots \pi^*$, $\pi \cdots \sigma^*$ interactions were also studied in complexes **3** and **4**.

Keywords: Rhenium(I) tricarbonyl; Diazabutadiene; NBO; Non-covalent interactions

1. Introduction

Transition metal carbonyl complexes have become one of the most important classes of coordination compounds in inorganic chemistry. These complexes are not only a subject of interest for basic synthesis and study in academic research but are also very important as homo- and heterogeneous catalysts in industry. The chemical bonding in transition metal carbonyl complexes themselves, or in metal carbonyl bearing diimine ligands, is based on the classical concept of synergistic σ -donation and π -back donation between the ligand (carbonyl or diimine) and the metal, introduced by Dewar-Chatt-Duncanson in 1951. An understanding of such properties of transition metal carbonyl complexes helps produce required knowledge of the properties of the molecular orbitals, spectra, and appropriate excited states [1]. Among different metal carbonyl complexes, Re(I)-tricarbonyl complexes with diimine ligands of the type $[\text{Re}(\text{CO})_3(\alpha\text{-diimine})(\text{X})]^{0/+}$, in which X is a halide, bridging ligand, organic donor/acceptor, nitrogen donor or some other monodentate or ambidentate ligands, have been the subject of much attention, mainly because of their photophysical and photochemical properties [2–4] and their use in the photoreduction and electroreduction of CO_2 to CO [5,6], a key process in the conversion and storage of solar energy as a model in natural photosynthesis, and in supramolecular chemistry and catalysis [7–10]. The photo-behaviour of these complexes may be interpreted in terms of three types of excited states: metal-to-ligand charge transfer (MLCT) states, ligand-to-ligand charge transfer (LLCT)

states, and intra-ligand (IL) states [11–16]. On the other hand, the spectroscopic properties of the Re(I)-tricarbonyl complexes are ligand-dependent and can be tuned by changing the chelated diimine and/or axial ligands. As such, the quantitative description of the electronic properties of diimine ligands based on their σ -donation and π -back donation nature can clarify such properties. By changing the electronic and steric effects in the DAB ligands in their Ni(II) and Pd(II) complexes, they can be utilized as efficient catalysts in alkene polymerization [17,18]. The tuning of such electronic and steric effects has been examined before in some iminophenol complexes [19,20]. Besides all the aforementioned properties, one of the interesting features of metal carbonyl complexes is the presence of intra- and/or intermolecular $n \cdots \pi^*$ interactions, which were not the subject of much attention experimentally and theoretically until their importance was noticed by Echeverría [21]. Since its introduction by Burgi-Dunitz, the so-called Burgi-Dunitz trajectory in the geometrical reaction coordinates in the nucleophilic addition to carbonyl group, most of the studies were focused on organic and biological systems [22–32].

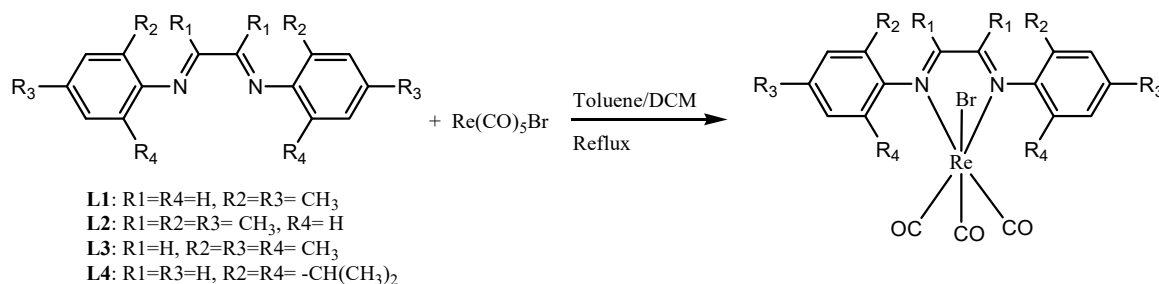
It has been demonstrated that $M\text{-CO}(\text{lone pair}) \cdots \pi$ interactions are relevant in the structures of a number of transition metal carbonyl complexes, and they have important effects on their internal geometry in the related complexes and supramolecular interactions of metal carbonyl complexes [33,34]. In spite of their inherently weak nature, $M\text{-CO}(\text{lone pair}) \cdots \pi^*$ interactions stabilize precise molecular conformations that maximize the overlap between the involved donor and acceptor orbitals in the interaction and can also provide a measure of stability to their crystal structures and lead to supramolecular architectures [35].

Therefore, the structural and computational studies of such interactions are of great interest and a new topic in the structural and computational chemistry of metal carbonyl complexes [36–38]. In continuation of our work on synthesis, characterization, structural chemistry, and computational studies of transition metal-carbonyl complexes [39,40], we here report the synthesis, spectroscopic, structural and computational studies of new Re(I)-tricarbonyl bromo complexes bearing 1,4-diazabutadiene as non-heterocyclic diimine ligands, namely: *N,N*-bis(2,4-dimethylbenzene)-1,4-diazabutadiene, ${}^{2,4\text{-Me}}_2\text{DAB}$ (1); *N,N*-bis(2,4-dimethylbenzene)-2,3-dimethyl-1,4-diazabutadiene, ${}^{2,4\text{-Me}}_2\text{DAB}^{\text{Me}}$ (2); *N,N*-bis(2,4,6-trimethylbenzene)-1,4-diazabutadiene, ${}^{2,4,6\text{-Me}}_3\text{DAB}$ (3); and *N,N*-bis(2,6-diisopropylbenzene)-1,4-diazabutadiene, ${}^{2,6\text{-ipr}}_2\text{DAB}$ (4). The solid-state structures of complexes 1–4 were confirmed by single-crystal X-ray diffraction, and the intra- and intermolecular interaction results from X-ray diffraction were elucidated by NCI and NBO calculations.

2. Experimental

2.1. General Methods

All chemicals used were analytical reagent grade. All solvents purchased from Merck were reagent grade and purified by standard techniques where required. CH_3CN was distilled over P_2O_5 for synthesis. Commercially available $\text{Re}(\text{CO})_5\text{Br}$ from Aldrich was used as received. The ${}^1\text{H}$ -NMR and ${}^{13}\text{C}$ -NMR (125 MHz) spectra were recorded using a BRUKER AVANCE 500 MHz spectrometer in CDCl_3 . IR spectra in the region of $4000\text{--}400\text{ cm}^{-1}$ were recorded in KBr pellets with a Shimadzu IRPrestige-21 FTIR spectrophotometer. Electronic absorption spectra were measured with a Rayleigh 5E spectrophotometer in dichloromethane solutions. The elemental analyses were done using a LECO CHNS instrument. The preparation of all Re(I) complexes (Scheme 1) was achieved using the previously reported procedure based on phenanthroline-type ligands, except that DAB ligands were used [41]. The FTIR, ${}^1\text{H}$ -NMR, and ${}^{13}\text{C}\{^1\text{H}\}$ -NMR spectra of the complexes are listed in the supplementary materials. The DAB ligands, L1–L4, were prepared by condensation of glyoxal or diacetyl with the appropriate primary amine, according to literature procedures (see Supporting Information) [42]. The analytical data on L1–L4 are shown in Figures S1–S8.



Scheme 1. Synthesis pathway of complexes 1–4.

[(^{2,4}-Me₂DAB)Re(CO)₃Br] (1). A mixture of Re(CO)₅Br (203 mg, 0.5 mmol) and ^{2,4}-Me₂DAB (132 mg, 0.5 mmol) in a mixture of CH₂Cl₂ (10 mL) and toluene (30 mL) was heated at reflux for 4 h to give a dark-brown solution. The volume of the solution was reduced to 10 mL and by addition of cold n-hexane the complex was precipitated. The crude material recrystallized from CH₂Cl₂/hexane to give the complex as a pure dark-brown microcrystalline powder. *Anal. Calc.* for C₁₃H₈BrN₂O₃Re: C, 41.05; H, 3.28; N, 4.56. Found: C, 41.04; H, 3.25, N, 4.58. ¹HNMR (δ_{ppm}, CDCl₃): 2.40 (s, 6H, 2-CH₃), 2.41 (s, 6H, 4-CH₃), 7.10–7.46 (m, 6H, aromatic protons), 8.61 (s, 2H, iminic protons). ¹³C{¹H}-NMR (125 MHz, CDCl₃): 18.06 (2-CH₃), 21.05 (4-CH₃), 123.14 (C6), 127.12 (C2), 127.55 (C5), 132.14 (C3), 138.64 (C4), 148.85 (C1), 165.02 (iminic carbon), 182.94 (CO_{ax}), 194.79 (CO_{eq}). IR (KBr, cm⁻¹): ν_{max} 2020 (CO_{ax}), 1938 and 1890 (CO_{eq}). UV–Vis in DCM: λ_{max} (ε): 230 (16750), 330 (3207), 394 (4387), 505 (3918).

[(^{2,4}-Me₂DAB^{Me})Re(CO)₃Br] (2). The complex was prepared by a procedure similar to **1** using 146 mg (0.5 mmol) of ^{2,4}-Me₂DAB^{Me}. The crude material recrystallized from CH₂Cl₂/hexane to give the complex as a pure dark-brown microcrystalline powder. *Anal. Calc.* for C₁₇H₁₂BrN₂O₃Re: C, 42.99; H, 3.76; N, 4.36. Found; C, 42.97; H, 3.75; N, 4.39. ¹HNMR (δ_{ppm}, CDCl₃): 2.10 (s, 6H, 2-CH₃), 2.20 (m, 6H, 4-(CH₃)), 2.35 (s, 6H, 7-CH₃), 7.0–7.5 (m, 6H, aromatic protons). ¹³C{¹H}-NMR (125 MHz, CDCl₃): 17.02 (2-CH₃), 20.41 (4-CH₃), 20.97 (7-CH₃), 121.37 (C6), 126.09 (C2), 128.36 (C5), 132.16 (C3), 137.31 (C4), 146.39 (C1), 174.97 (iminic carbon), 185.01 (CO_{ax}), 195.28 (CO_{eq}). IR (KBr, cm⁻¹): ν_{max} 2019 (CO_{ax}), 1825 and 1896 (CO_{eq}). UV–Vis in DCM: λ_{max}, (ε): 231 (36301), 460 (6571).

[(^{2,4,6}-Me₃DAB)Re(CO)₃Br] (3). The complex was prepared by a procedure similar to **1** using 146 mg (0.5 mmol) of ^{2,4,6}-Me₃DAB. The crude material recrystallized from CH₂Cl₂/hexane to give the complex as a pure dark-brown microcrystalline powder. *Anal. Calc.* for C₁₇H₁₂BrN₂O₃Re: C, 42.99; H, 3.76; N, 4.36. Found; C, 42.95; H, 3.77; N, 4.38. ¹HNMR (δ_{ppm}, CDCl₃): 2.28 (s, 6H, 6-CH₃), 2.37 (s, 6H, 2-CH₃), 2.60 (s, 6H, 4-CH₃), 7.0–7.28 (m, 4H, aromatic protons), 8.69 (s, 2H, iminic protons). ¹³C{¹H}-NMR (125 MHz, CDCl₃): 19.03 (6-CH₃), 20.77 (2-CH₃), 20.89 (4-CH₃), 128.29 (C6), 129.64 (C5), 129.94 (C2), 130.25 (C3), 137.97 (C4), 148.44 (C1), 165.88 (iminic carbon), 183.89 (CO_{ax}), 194.17 (CO_{eq}). IR (KBr, cm⁻¹): ν_{max} 2026 (CO_{ax}), 1936 and 1895 (CO_{eq}). UV–Vis in DCM: λ_{max} (ε): 233 (18406), 328 (2726), 400 (3847), 512 (5325).

[(^{2,6}-iPr₂DAB)Re(CO)₃Br] (4). The complex was prepared by a procedure similar to **1** using 188 mg (0.5 mmol) of ^{2,6}-iPr₂DAB. The crude material recrystallized from CH₂Cl₂/hexane to give the complex as a pure dark-brown microcrystalline powder. *Anal. Calc.* for C₁₇H₁₂N₃O₅Re: C, 47.93; H, 4.99; N, 3.85. Found; C, 47.80; H, 4.97; N, 3.87. ¹HNMR (δ_{ppm}, CDCl₃): 1.1 (m, 12H, 8-(CH₃)₂), 1.35 (m, 12H, 9-(CH₃)₂), 2.75 (m, 2H, isopropyl protons (8-CH)), 4 (m, 2H, isopropyl protons (9-CH)), 7.1–7.4 (m, 6H, aromatic protons), 8.7 (s, 2H, iminic protons). ¹³C{¹H}-NMR (125 MHz, CDCl₃): 23.18 and 26.44 and 27.08 and 28.38 (methyl groups), 28.55 (isopropyl carbon), 124.19 (C5), 124.91 (C3), 129.09 (C4), 139.54 (C6), 141.01 (C2), 148.14 (C1), 166.22 (iminic carbon), 182.58 (CO_{ax}), 194.19 (CO_{eq}). IR (KBr, cm⁻¹): ν_{max} 2027 (CO_{ax}), 1930 (CO_{eq}). UV–Vis in DCM: λ_{max} (ε): 229 (9909), 332 (1295), 516 (3213).

2.2. X-ray Crystallography

Single crystals of **1–4**, suitable for X-ray diffraction analysis, were grown by slow vapor diffusion of n-hexane into a dichloromethane solution of the complexes. X-ray intensity data were collected

using the full-sphere routine by φ and ω scans strategy on the Agilent *SuperNova* dual wavelength EoS S2 diffractometer with mirror monochromated Mo $K\alpha$ radiation ($\lambda = 0.71073 \text{ \AA}$) for **1**, **2**, and **4** and with Cu $K\alpha$ radiation for **3**. For all data collections, the crystals were cooled to 150(2) K using an Oxford diffraction Cryojet low-temperature attachment. The data reduction, including an empirical absorption correction using spherical harmonics, implemented in the *SCALE3 ABSPACK* scaling algorithm, was performed using the *CrysAlisPro* software package [43]. The crystal structures of **1–4** were solved by direct methods using the online version of *AutoChem 2.0* in conjunction with the *OLEX2* suite of programs [44] implemented in the *CrysAlis* software, and then refined by full-matrix least-squares (*SHELXL-2018*) on F^2 [45]. The non-hydrogen atoms were refined anisotropically. All of the hydrogen atoms were positioned geometrically in idealized positions and refined with the riding model approximation, with $U_{\text{iso}}(\text{H}) = 1.2$ or $1.5 U_{\text{eq}}(\text{C})$. For the molecular graphics, the program *SHELXTL* was used [45]. All geometric calculations were carried out using the *PLATON* software [46]. The full crystal data, bond lengths and angles are listed in the supplementary materials.

2.3. Computational Details

Density functional theory (DFT) calculations have been performed using the *Gaussian09* package [47] to perform geometry optimizations for vibrational frequencies and electronic structures of complexes **1–4**. The structures of all complexes were optimized using the computational model (PBE1PBE) by combining the Perdew–Burke–Erzenrhof with the quasi-relativistic Stuttgart–Dresden (SDD) effective core pseudopotential (ECP) and corresponding set of basic functions for the Re atom and 6-31G* (five pure d functions) for C, H, N, O, and 6-311+G* for Br [48,49].

3. Results and Discussion

3.1. Synthesis and Characterization

The new [(NN)Re(CO)₃X] (NN = diazabutadiene) complexes were synthesized via substitution reaction from the DAB ligands and Re(CO)₅Br in a mixture of CH₂Cl₂ and toluene under reflux condition. Complexes **1–4** were recrystallized from a mixture of CH₂Cl₂/*n*-hexane, and the purity of all complexes was confirmed by elemental analyses. The characteristic feature of the complexes incorporating *fac*-[Re(CO)₃]⁺ by losing two carbonyl groups in *cis* positions is the appearance of three intense carbonyl bands at about 2050–1880 cm⁻¹, including a sharp intense band at about 2030–2050 cm⁻¹ and two closely spaced lower energy bands consistent with the A'(cis), A''(cis), and A'(trans) modes expected in C_s symmetry, with energy ordering A'(cis) > A''(cis) > A'(trans) as reported by Cotton-Karihanzel based on force field calculation [50–52]. As a normal trend, the position of the absorption bands is influenced by the electronic nature of the axial ligand. Normally, with the weakly donating ligands in the axial position, the $\nu(\text{CO})$ is further increased. The electronic nature of the axial ligand (X) in *fac*-Re(CO)₃(NN)(X) complexes influences merging or splitting of the lower energy bands of the carbonyl groups. A stronger π -acceptor ligand in the basal plane shifts the CO stretching bands to higher frequencies. For complexes **2** and **4**, by merging two lower energy bands, there seems to be an approximate C_{3v} spectroscopic symmetry, leading to a virtual "E" band. The FT-IR spectra of complexes **1–4** are shown in Figures S9–S12. The stretching frequencies of the complexes are listed in the experimental section. The ¹H-NMR and ¹³C{¹H}-NMR spectra of complexes **1–4** are shown in Figures S13–S20.

3.2. X-ray Crystal Structures

The solid-state structures of complexes **1–4** were determined by X-ray crystallography and are shown with their atom labelling scheme in Figure 1. Details of data collection and refinement parameters are given in Table 1. Selected bond lengths and angles for complexes **1–4** are listed in Table 2. The details of the hydrogen bonding interactions are listed in Table 3.

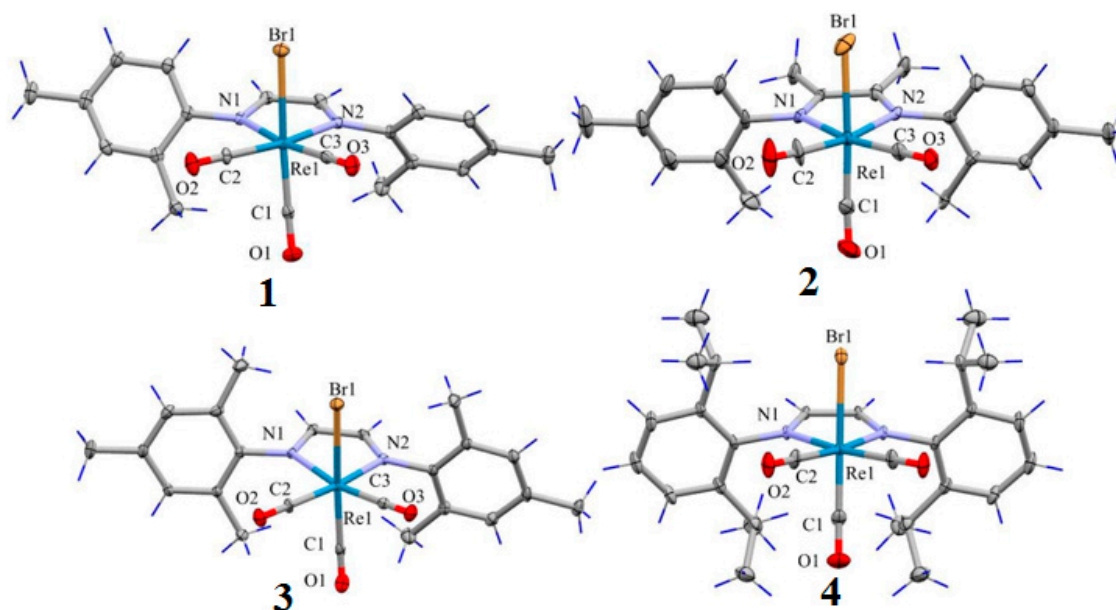


Figure 1. The molecular structure of complexes 1–4, showing 40% probability displacement ellipsoids and the atomic numbering (H atoms are shown as blue wire). The symmetry code for unlabeled atoms in 4 is $x, -y+1/2, z$.

Table 1. Crystal data and refinement parameters of complexes 1–4.

Complex	1	2	3	4
Empirical Formula	$C_{21}H_{20}BrN_2O_3Re$	$C_{23}H_{24}BrN_2O_3Re$	$C_{23}H_{24}N_2O_3Re$	$C_{29}H_{36}BrN_2O_3Re$
Formula Mass	614.50	642.55	642.55	726.71
Crystal Size (mm)	$0.10 \times 0.15 \times 0.25$	$0.04 \times 0.08 \times 0.15$	$0.10 \times 0.18 \times 0.35$	$0.10 \times 0.18 \times 0.35$
Colour	Dark-brown	Dark-brown	Dark-brown	Dark-red
Crystal System	Monoclinic	Triclinic	Orthorhombic	Orthorhombic
Space Group	$P2_1/n$	$P-1$	$Pbca$	$Pnma$
θ_{max} (°)	26	30.4	72.9	29.4
a (Å)	7.3182(2)	8.1105(3)	14.0730(2)	13.3103(5)
b (Å)	21.8786(9)	8.3373(4)	13.8361(2)	21.7931(9)
c (Å)	13.0930(5)	18.3651(11)	23.2653(3)	10.3165(5)
α (°)	90	93.857(4)	90	90
β (°)	95.658(3)	97.380(4)	90	90
γ (°)	90	104.588(4)	90	90
V (Å ³)	2086.13(13)	1185.41(10)	4530.11(11)	2992.5(2)
Z	4	2	8	4
D_{calc} (Mg/m ³)	1.957	1.800	1.884	1.613
μ (mm ⁻¹)	7.764	6.836	12.775	5.462
$F(000)$	1176	620	2480	1432
Index Ranges	$-9 \leq h \leq 8$ $-26 \leq k \leq 26$ $-17 \leq l \leq 16$	$-11 \leq h \leq 11$ $-11 \leq k \leq 11$ $-25 \leq l \leq 25$	$-17 \leq h \leq 11$ $-14 \leq k \leq 17$ $-28 \leq l \leq 28$	$-18 \leq h \leq 15$ $-27 \leq k \leq 18$ $-13 \leq l \leq 8$
No. of Measured Reflins.	16734	23113	21739	8882
No. of independent reflns./ R_{int}	4084/0.046	6361/0.067	4448/0.03	3587/0.047
No. of observed reflns. $I > 2\sigma(I)$	3477	5247	4228	2868
No. of parameters	1.07	1.18	1.13	1.02
Goodness-of-fit (GOF)	0.0261	0.0783	0.0288	0.0377
R_1 (observed data)	0.0574	0.1694	0.0726	0.0722
wR_2 (all data)				

Table 2. Selected bond lengths (Å) and angles (°) of 1–4.

Bond Lengths (Å)	1	2	3	4
Re(1)–N(1)	2.180(3) [2.175] ^a	2.169(9) [2.173]	2.182(3) [2.209]	2.176(3) [2.223]
Re(1)–N(2)	2.150(4) [2.188]	2.159(9) [2.173]	2.179(3) [2.182]	-
Re(1)–C(1)	2.6114(6) [1.916]	1.870(14) [1.911]	1.994(4) [1.914]	1.893(7) [1.927]
Re(1)–C(2)	1.933(4) [1.935]	1.922(16) [1.936]	1.934(4) [1.938]	1.918(4) [1.951]
Re(1)–C(3)	1.923(4) [1.936]	1.921(13) [1.936]	1.924(4) [1.932]	-
C(1)–O(1)	1.141(5) [1.161]	1.167(19) [1.163]	1.002(6) [1.162]	1.166(9) [1.165]
C(2)–O(2)	1.142(5) [1.156]	1.15(2) [1.157]	1.142(5) [1.156]	1.148(5) [1.159]
C(3)–O(3)	1.141(5) [1.157]	1.135(17) [1.157]	1.145(5) [1.157]	-
Re(1)–Br(1)	2.6114(6) [2.655]	2.6166(18) [2.668]	2.6161(5) [2.664]	2.6122(7) [2.712]
Bond Angles (°)				
N(1)–Re(1)–N(2)	74.59(13) [74.03]	73.3(4) [72.98]	74.08(11) [74.11]	75.62(12) [73.92]
C(1)–Re(1)–N(1)	99.20(14) [92.51]	95.5(5) [95.11]	99.86(14) [98.94]	96.53(18) [97.10]
C(2)–Re(1)–N(2)	169.99(15) [170.0]	171.2(6) [170.04]	171.19(15) [171.16]	-
N(1)–Re(1)–C(3)	171.97(16)	168.9(5) [170.05]	169.73(14) [168.91]	-
N(2)–Re(1)–C(3)	[170.22]	95.4(8) [98.08]	99.32(15) [97.47]	-
C(1)–Re(1)–C(3)	99.45(15) [96.54]	89.6(6) [89.98]	88.05(17) [88.38]	-
C(2)–Re(1)–C(3)	86.35(17) [91.24]	89.1(6) [90.44]	89.49(18) [91.17]	-
C(1)–Re(1)–Br(1)	90.09(16) [90.51]	177.7(4) [179.19]	173.55(12) [174.76]	176.1(2) [170.9]

^a The values in bracket are from theoretical calculations.**Table 3.** Hydrogen bonding interaction parameters in complexes 1–4.

	D–H...A	H...A (Å)	D...A (Å)	D–H...A (°)
Complex 1	C(11)–H(11) ... Br(1) ⁱ	2.75	3.629(4)	158
Complex 2	C(13)–H(16) ... Br(1) ⁱⁱ	2.92	3.841(12)	168
Complex 3	C(11)–H(11) ... O(1) ⁱⁱⁱ	2.45	3.375(6)	162
	C(20)–H(20B) ... Br(1)	2.65	3.572(5)	162
	C(21)–H(21A) ... O(1)	2.51	3.303(6)	140
	C(23)–H(23C) ... Br(1)	2.78	3.681(5)	156
Complex 4	C(6)–H(6) ... O(2) ^{iv}	2.52	3.451(6)	177
	C(10)–H(10) ... Br(1)	2.62	3.564(4)	163

Symmetry codes: (i) 1 - x, 1 - y, 1 - z (ii) 1 + x, 1 + y, z (iii) $\frac{1}{2} + x, \frac{1}{2} - y, -1/2 + z$ (iv) 1 - x, $\frac{1}{2} + y, -1 - z$.

The geometry around the Re(I) is a distorted octahedron involving the carbonyl groups in *facial* arrangement, a DAB ligand and axial bromo group. In complex 2, the methyl group in the *ortho* position was disordered over two positions with a refined site-occupancy ratio of 0.81(2)/0.19(2). The most significant angular distortion is associated with the bite angles of the DAB ligands N(1)–Re(1)–N(2) in the range of 73.3(4)–75.62(12)° which is due to the formation of the strained five-membered chelate ring. The *trans* angle C(1)–Re(1)–Br(1) in 1–4 falls in the range of 173.55(12)–177.7(4)°, respectively. The bond lengths, angles and coordination geometry of the crystal structures in 1–4 are similar to those structures reported previously [53,54]. There is only one report related to the crystal structure of 1,4-alkyldiazabutadiene, namely 1,4-di(*tert*-butyl) diazabutadiene, which shows significantly different Re–N [2.170(15), 2.226(19) Å], C≡O [1.13(3), 1.16(3), and 1.01(3) Å] bond lengths compared to 1,4-aryldiazabutadiene, but the Re–Br bond length is similar to complexes 1–4 [13]. The interesting feature of complexes 1 and 3 is the intermolecular n ... π* interactions which connects neighbouring molecules into a 1-D extended chain along the *a*- and *b*-axis, respectively (Figures 2 and 3). As it is summarized in Table 3, the crystal packing of the complexes is consolidated mainly by the intermolecular non-classic C–H ... O and C–H ... Br hydrogen bonding. In complexes 1 and 4, the intermolecular C–H ... Br and C–H ... O interactions form individual dimers in the crystal packing, respectively. In case of complexes 2 and 3, intermolecular C–H ... Br and C–H ... O interactions connect neighbouring molecules into an extended infinite chain along the *b*-axis, respectively. Figure 4 shows

one-dimensional extended chain formation along the *a*-axis through intermolecular C–H···O and C–H···Br interactions in complex 4.

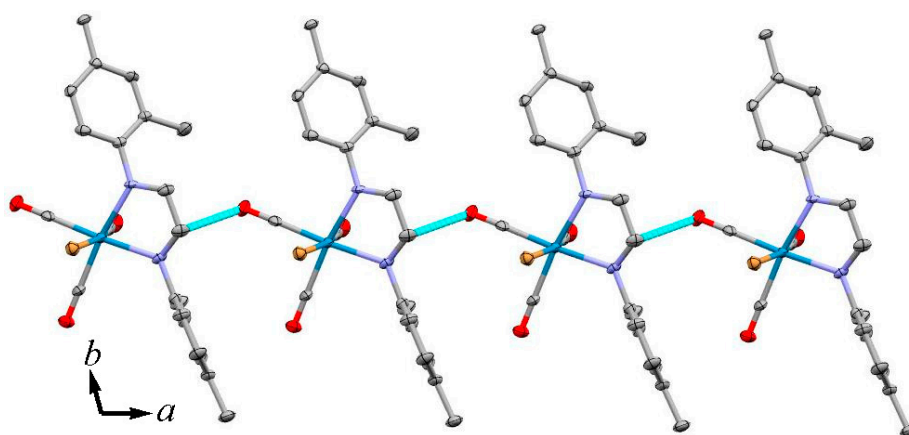


Figure 2. Part of the crystal packing of 1, showing one-dimensional extended chain formation along the *a*-axis through intermolecular n→π* interaction (H atoms omitted for clarity).

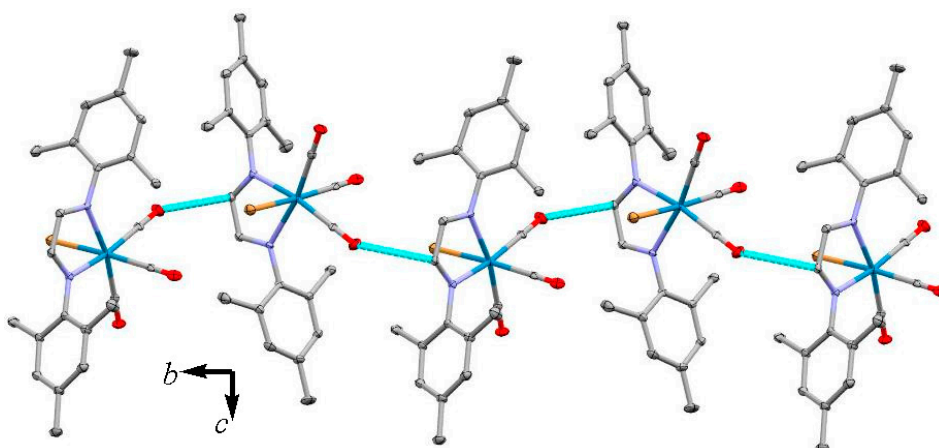


Figure 3. Part of the crystal packing of 3, showing one-dimensional extended chain formation along the *b*-axis through intermolecular n→π* interaction (H atoms omitted for clarity).

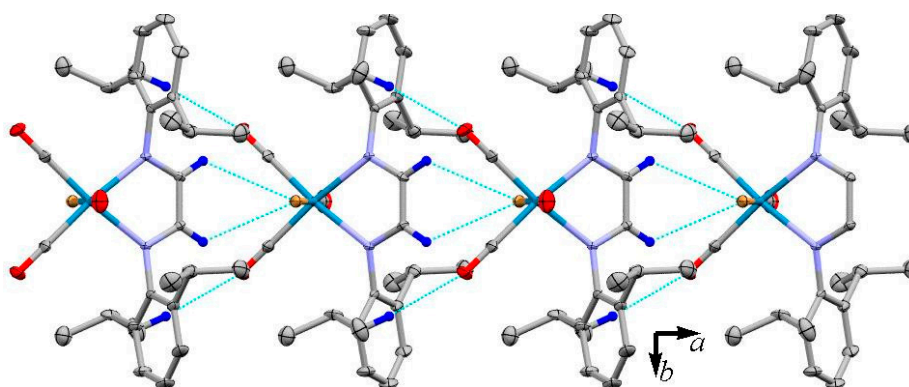


Figure 4. Part the crystal packing of 4, showing one-dimensional extended chain formation along the *a*-axis through intermolecular C–H···O and C–H···Br interaction (H atoms omitted for clarity).

3.3. Non-Covalent Interaction Index and Natural Bond Orbitals (NBOs)

Non-covalent interactions were evaluated using the non-covalent index (NCI) approach, which relies on the topological analysis of the electron density and its derivatives at low density regions based

on the reduced density gradient (RDG) [55,56]. The NCI isosurface regions show both stabilizing and destabilizing weak interactions. These are distinguishable according to the total sign of the second eigenvalue of the Hessian (λ_2) matrix, where the sign of the λ_2 quantity can vary accordingly and are thus suggested as a useful descriptor to characterize such situations. Negative values of the product given by $\rho^* \text{sign}(\lambda_2)$, denote stabilizing interactions. Values close to zero account for weak interactions (van der Waals forces), while positive values account for weak repulsive cases. One of the main reasons to include the Br ligand in the axial position of the complexes was to increase the possibility of intra- and intermolecular interactions through halogen \cdots halogen and halogen \cdots oxygen bonding, since Br has a greater tendency to act as halogen bond acceptor compared to Cl, because of the greater σ -hole [57]. Complexes **1**, **3**, and **4** showed some interesting intra- and intermolecular interactions which were investigated by non-covalent interaction index (NCI) and NBO calculations. The NCI analyses for single molecules were done based on the optimized structures, but in case of the dimer pairs they were calculated directly from the crystallographically generated dimers without optimization. The surface NCI analyses are depicted in Figures 5–8, revealing stabilizing weak non-covalent intramolecular interactions in single-molecule and intermolecular interactions between interacting pairs, respectively. On the other hand, to shed light on the nature and strength of the intra- and intermolecular interactions depicted by NCI calculations, NBO analysis of other suitable descriptors for bond analysis was used with more details. Natural bond orbital calculations were performed on **1**, **3**, and **4** with the same level of theory for molecular orbital calculations [58]. The NBO analysis shows that the attractive nature is associated with donor–acceptor orbital interactions in single molecules and between the pairs. Figure 5 shows the intermolecular interactions in **1** with contributions from the lone pair of oxygen in the carbonyl group and the π^* of the imine functional group, $n_s(\text{O}3) \cdots \pi^*(\text{C}10=\text{N}1)$ and $\pi(\text{C}3=\text{O}3) \cdots \pi^*(\text{C}10=\text{N}1)$, with $0.47 \text{ kcal mol}^{-1}$ according to the NBO analysis from second-order perturbation energy. The energy contribution of $n_s(\text{O}2) \cdots \pi^*(\text{C}8=\text{C}9)$ was negligible.

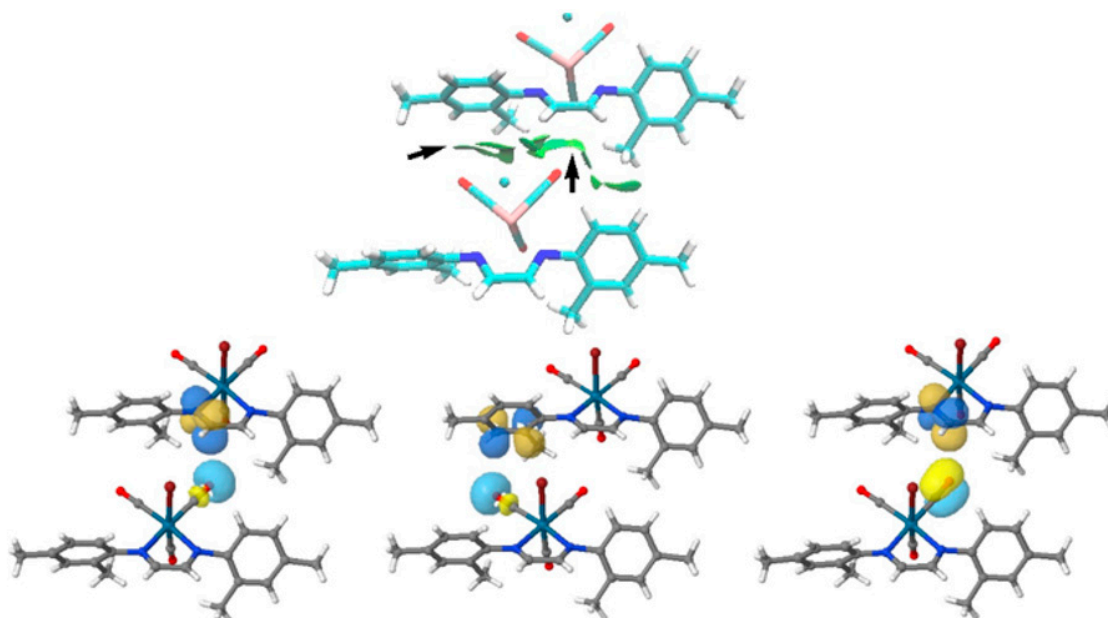


Figure 5. NCI plot of interacting dimer in **1** and the donor–acceptor interacting orbitals from NBO calculations. The area of $n \cdots \pi^*$ and $\pi \cdots \pi^*$ are shown in the NCI plot with arrows.

The NCI plot and NBO analyses of **3** are shown in Figure 6. The NCI plot shows interactions between the C–H bond of the methyl group and Br [A–H] and the C–H bond and the carbonyl group, I–L, in axial positions with light-blue color, confirming attractive interactions. These interactions are due to the overlap of the perpendicular occupied s and p orbitals of Br to the empty σ^* orbital of the C–H bond with overall energy release of $8.07 \text{ kcal mol}^{-1}$, based on the NBO analysis from

second-order perturbation energy. The contribution from $n_p(\text{Br}) \cdots \sigma^*(\text{C}-\text{H})$, C-D, was 2.48, 2.27, and 2.09 kcal mol⁻¹, respectively.

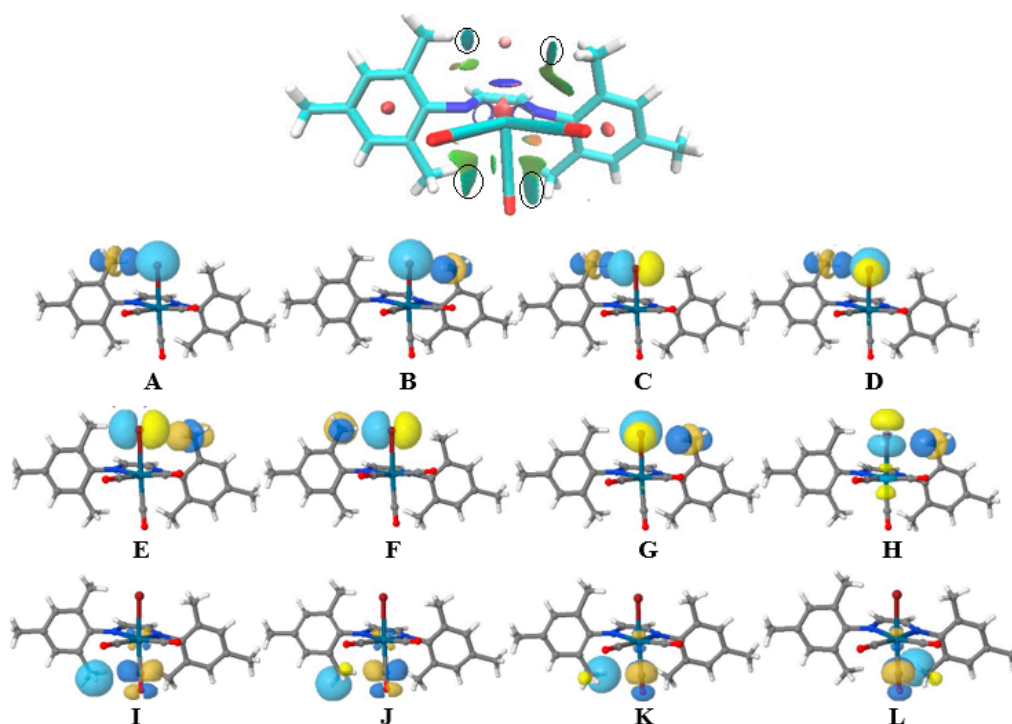


Figure 6. NCI plot of **3** and the representation of interacting donor–acceptor $n_s(\text{Br}) \cdots \sigma^*(\text{CH})$, A–B; $n_p(\text{Br}) \cdots \sigma^*(\text{CH})$, C–H; $\sigma(\text{CH}) \cdots \pi^*(\text{CO})$, I–L; orbitals from NBO calculations.

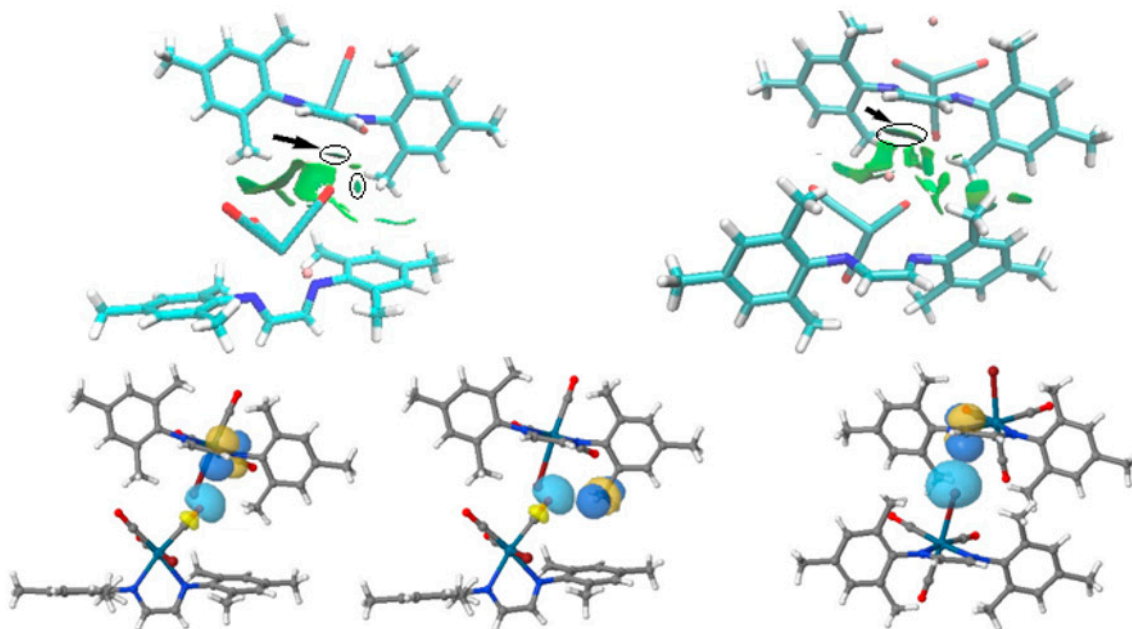


Figure 7. NCI plot of the interacting dimer in **3** and the representation of donor–acceptor interacting $n(\text{O}) \cdots \pi^*$, $n(\text{O}) \cdots \sigma^*$, and $n(\text{Br}) \cdots \pi^*$ orbitals from NBO calculations. The area is shown in the NCI plot with arrows.

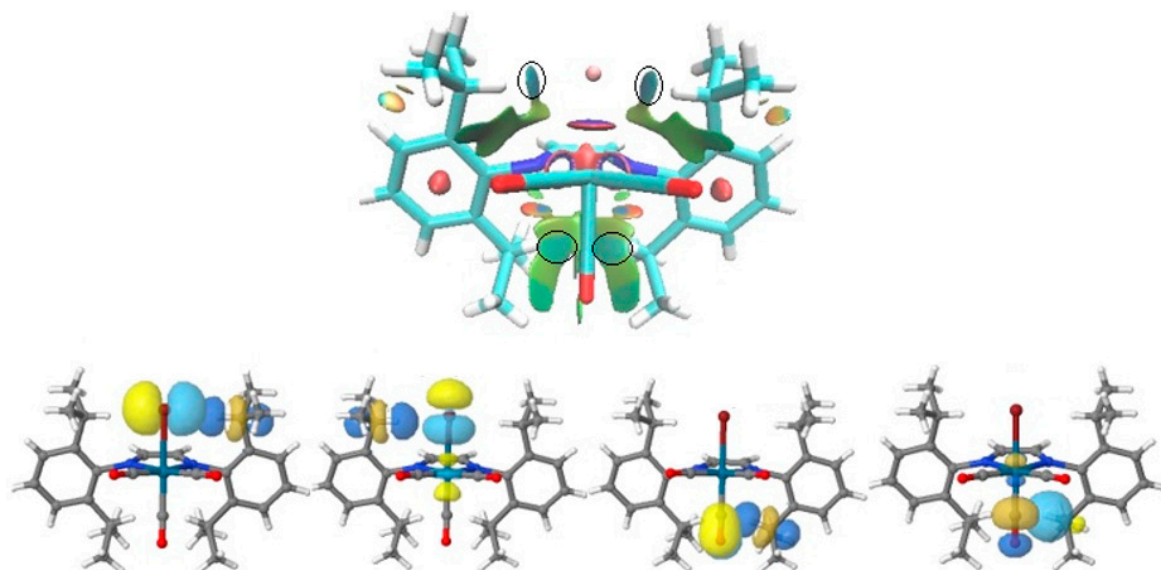


Figure 8. NCI plot of interacting dimer in **4** and the donor–acceptor interacting orbitals from NBO calculations through $n_p(\text{Br}) \cdots \sigma^*$, $n_p(\text{Br}) \cdots \sigma^*$, $\pi(\text{CO}) \cdots \sigma^*$, $\sigma \cdots \pi^*(\text{CO})$ from left to right, respectively. The interaction area is shown with black circles.

On the other hand, the NCI plot and NBO calculations of the interaction pairs of **3** were also analyzed and depicted in Figure 7. The total energy release of the $n(\text{O}) \cdots \pi^*$ and $n(\text{O}) \cdots \sigma^*$ was $0.68 \text{ kcal mol}^{-1}$, while the contribution from $n(\text{Br}) \cdots \pi^*$ was $0.31 \text{ kcal mol}^{-1}$ based on second-order perturbation energy calculations.

The NCI plot and NBO analyses of **4** are shown in Figure 8. The NCI plot shows some intramolecular interactions among the Br, isopropyl and CO groups with green-blue color, confirming attractive interaction. The NBO study confirms the $n_p(\text{Br}) \cdots \sigma^*$, $\pi(\text{CO}) \cdots \sigma^*$, and $\sigma \cdots \pi^*(\text{CO})$ interactions in **4** with energy releases of 3.46 , 0.28 and $0.44 \text{ kcal mol}^{-1}$ based on the NBO analysis from second-order perturbation energy, respectively.

4. Conclusions

In this paper, we have described the synthesis, characterization, structural and full computational studies of four bromide- tricarbonyl Re(I) complexes **1–4**, bearing substituted diazabutadiene ligands. The molecular structures of the complexes were established by single-crystal X-ray diffraction, feature the metal in a distorted octahedral environment with *facial* arrangement of the carbonyl groups in the complexes, which was also confirmed by FT-IR spectroscopy. The nature and energy of the intermolecular $n(\text{O}) \cdots \pi^*$ interactions between carbonyl-bound metal and π^* of benzene ring and imine segments in **1** and $n(\text{O}) \cdots \pi^*$ and $n(\text{Br}) \cdots \pi^*$ in **3** were investigated in detail. The presence of such interactions was also confirmed by NCI index based on colour codes. The complexes **3** and **4** showed interesting intramolecular $n_p(\text{Br}) \cdots \sigma^*$ interactions, which stabilized the internal geometry of the coordinated ligand around the metal center.

Supplementary Materials: The following are available online at <http://www.mdpi.com/2073-4352/10/4/267/s1>. CCDC 1962581(1), 1962582(2), 1962583(3), and 1962580(4) contain the supplementary crystallographic data for this paper. These data can be obtained free of charge from The Cambridge Crystallographic Data Centre via www.ccdc.cam.ac.uk/data_request/cif. FT-IR of complexes **1–4**, the crystal packing of complexes **1–4**, some of the important frontier molecular orbitals of **5**, and crystallographic data of complexes **1–4** in CIF format. Figure S1. The $^1\text{H-NMR}$ spectrum of complex **L1**; Figure S2. The $^{13}\text{C}\{^1\text{H}\}$ -NMR spectrum of complex **L1**; Figure S3. The $^1\text{H-NMR}$ spectrum of complex **L2**; Figure S4. The $^{13}\text{C}\{^1\text{H}\}$ -NMR spectrum of complex **L2**; Figure S5. The $^1\text{H-NMR}$ spectrum of complex **L3**; Figure S6. The $^{13}\text{C}\{^1\text{H}\}$ -NMR spectrum of complex **L3**; Figure S7. The $^1\text{H-NMR}$ spectrum of complex **L4**; Figure S8. The $^{13}\text{C}\{^1\text{H}\}$ -NMR spectrum of complex **L4**; Figure S9. The FTIR spectrum of **1** in KBr pellet; Figure S10. The FTIR spectrum of **2** in KBr pellet; Figure S11. The FTIR spectrum of **3** in KBr pellet; Figure S12. The FTIR spectrum of **4** in KBr pellet; Figure S13. The $^1\text{H-NMR}$ spectrum of complex

1; Figure S14. The $^{13}\text{C}\{^1\text{H}\}$ -NMR spectrum of complex 1; Figure S15. The ^1H -NMR spectrum of complex 2; Figure S16. The $^{13}\text{C}\{^1\text{H}\}$ -NMR spectrum of complex 2; Figure S17. The ^1H -NMR spectrum of complex 3; Figure S18. The $^{13}\text{C}\{^1\text{H}\}$ -NMR spectrum of complex 3; Figure S19. The ^1H -NMR spectrum of complex 4; Figure S20. The $^{13}\text{C}\{^1\text{H}\}$ -NMR spectrum of complex 4.

Author Contributions: Manuscript preparation, X-ray structure determination, final structure analysis, and final editing of manuscript: R.K.; Synthesis and spectroscopic characterization of the complexes, manuscript review A.K. All authors have read and agreed to the published version of the manuscript.

Funding: This research was funded by Sharif University of Technology Research Council for financial support.

Conflicts of Interest: The funder had no role in the design of the study and in the decision to publish the results.

References

1. Ehlers, A.W.; Dapprich, S.; Vyboishchikov, S.F.; Frenking, G. Structure and Bonding of the Transition-Metal Carbonyl Complexes $\text{M}(\text{CO})_5\text{L}$ ($\text{M} = \text{Cr}, \text{Mo}, \text{W}$) and $\text{M}(\text{CO})_3\text{L}$ ($\text{M} = \text{Ni}, \text{Pd}, \text{Pt}$; $\text{L} = \text{CO}, \text{SiO}, \text{CS}, \text{N}_2, \text{NO}^+, \text{CN}^-, \text{NC}^-, \text{HCCH}, \text{CCH}_2, \text{CH}_2, \text{CF}_2, \text{H}_2$). *Organometallics* **1996**, *15*, 105–117. [[CrossRef](#)]
2. Lee, A.J. Luminescence properties of organometallic complexes. *Chem. Rev.* **1987**, *87*, 711–743.
3. Farrell, I.R.; Vlcek, A., Jr. Mechanisms of ultrafast metal–ligand bond splitting upon MLCT excitation of carbonyl-diimine complexes. *Coord. Chem. Rev.* **2000**, *208*, 87–101. [[CrossRef](#)]
4. Striplin, D.R.; Crosby, G.A. Photophysical investigations of rhenium(I)Cl(CO)₃(phenanthroline) complexes. *Coord. Chem. Rev.* **2001**, *211*, 163–175. [[CrossRef](#)]
5. Collin, J.P.; Sauvage, J.P. Electrochemical reduction of carbon dioxide mediated by molecular catalysts. *Coord. Chem. Rev.* **1989**, *93*, 245–268. [[CrossRef](#)]
6. Rossenaar, B.R.; Hartl, F.; Stufkens, D.J. Reduction of $[\text{Re}(\text{X})(\text{CO})_3(\text{R}'\text{-DAB})]$ ($\text{X} = \text{Otf}^-, \text{Br}^-$; $\text{DAB} = \text{Diazabutadiene}$; $\text{R}' = \text{iPr}, \text{pTol}, \text{pAn}$) and $[\text{Re}(\text{R})(\text{CO})_3(\text{iPr-DAB})]$ ($\text{R} = \text{Me}, \text{Et}, \text{Bz}$) Complexes: A Comparative (Spectro)electrochemical Study at Variable Temperatures. *Inorg. Chem.* **1996**, *35*, 6194–6203. [[CrossRef](#)]
7. Balzani, V.; Juris, A.; Venturi, M.; Campagna, S.; Serroni, S. Luminescent and Redox-Active Polynuclear Transition Metal Complexes. *Chem. Rev.* **1996**, *96*, 759–834. [[CrossRef](#)]
8. Slone, R.V.; Hupp, J.T. Synthesis, Characterization, and Preliminary Host–Guest Binding Studies of Porphyrinic Molecular Squares Featuring fac-Tricarbonylrhenium(I) Chloro Corners. *Inorg. Chem.* **1997**, *36*, 5422–5423. [[CrossRef](#)]
9. Nieto, S.; Perez, J.; Riera, L.; Riera, V.; Miguel, D. Non-covalent interactions between anions and a cationic rhenium diamine complex: Structural characterization of the supramolecular adducts. *New J. Chem.* **2006**, *30*, 838–843. [[CrossRef](#)]
10. Hevia, E.; Perez, J.; Riera, V.; Miguel, D.; Kassel, S.; Rheingold, A.L. New Synthetic Routes to Cationic Rhenium Tricarbonyl Bipyridine Complexes with Labile Ligands. *Inorg. Chem.* **2002**, *41*, 4673–4679. [[CrossRef](#)]
11. Machura, B.; Wolff, M.; Jaworska, M.; Lodowski, P.; Benoist, E.; Carrayon, C.; Saffon, N.; Kruszynski, R.; Mazurak, Z. Rhenium(I) carbonyl complex of 4,7-diphenyl-1,10-phenanthroline—Spectroscopic properties, X-Ray structure, theoretical studies of ground and excited electronic states. *J. Organomet. Chem.* **2011**, *696*, 3068–3075. [[CrossRef](#)]
12. Drozd, A.; Bubrin, M.; Fiedler, J.; Zalis, S.; Kaim, W. (α -Diimine)tricarbonylhalorhenium complexes: The oxidation side. *Dalton Trans.* **2012**, *41*, 1013–1019. [[CrossRef](#)] [[PubMed](#)]
13. Grupp, A.; Bubrin, M.; Ehret, F.; Kvapilova, H.; Zalis, S.; Kaim, W. Oxidation and reduction response of α -diimine complexes with tricarbonylrhenium halides and pseudohalides. *J. Organomet. Chem.* **2014**, *751*, 678–685. [[CrossRef](#)]
14. Kumar, A.; Sun, S.-S.; Lees, A.J. Photophysics and Photochemistry of Organometallic Rhenium Diimine Complexes. *Top. Organomet. Chem.* **2010**, *29*, 1–35.
15. Kirgan, R.A.; Sullivan, B.P.; Rillema, D.P. Photochemistry and Photophysics of Coordination Compounds: Rhenium. *Top. Curr. Chem.* **2007**, *281*, 45–100.
16. Kinghat, R.; Khatyr, A.; Knorr, M.; Kubicki, M.M.; Vigier, E.; Villafañe, F. Mono- and di-nuclear 2,3-diazabutadiene and 2-azabutadiene complexes of Rhenium(I): Syntheses, luminescence spectra and X-ray structures. *Inorg. Chem. Commun.* **2008**, *11*, 1060. [[CrossRef](#)]
17. Zou, W.; Chen, C. Influence of Backbone Substituents on the Ethylene (Co)polymerization Properties of α -diimine Pd(II) and Ni(II) Catalysts. *Organometallics* **2016**, *35*, 1794–1801. [[CrossRef](#)]

18. Kong, S.; Song, K.; Liang, T.; Guo, C.-Y.; Sun, W.-H.; Redshaw, C. 18 Methylene-bridged bimetallic α -diimino nickel(II) complexes: Synthesis and high efficiency in ethylene polymerization. *Dalton Trans.* **2013**, *42*, 9176–9178. [[CrossRef](#)]
19. Abakumov, G.A.; Druzhkov, N.O.; Egorova, E.N.; Kocherova, T.N.; Shavyrin, A.S.; Cherkasov, A.V. Intramolecular cyclization–decyclization of new sterically hindered diiminophenol. Synthesis and coordination abilities. *RSC Adv.* **2014**, *4*, 14495–14500. [[CrossRef](#)]
20. Egorova, E.N.; Druzhkov, N.O.; Shavyrin, A.S.; Cherkasov, A.V.; Abakumova, G.A.; Fedorov, A.Y. The group 13 metal complexes of sterically hindered substituted iminophenol: Synthesis and structure. *RSC Adv.* **2015**, *5*, 19362–19367. [[CrossRef](#)]
21. Echeverría, J. The $n \rightarrow \pi^*$ interaction in metal complexes. *Chem. Commun.* **2018**, *54*, 3061–3064. [[CrossRef](#)] [[PubMed](#)]
22. Burgi, H.B.; Dunitz, J.D.; Lehn, J.M.; Wipff, G. Stereochemistry of reaction paths at carbonyl centres. *Tetrahedron* **1974**, *30*, 1563–1572. [[CrossRef](#)]
23. Burgi, H.B.; Dunitz, J.D.; Shefter, E. Geometrical reaction coordinates. II. Nucleophilic addition to a carbonyl group. *J. Am. Chem. Soc.* **1973**, *95*, 5065–5067. [[CrossRef](#)]
24. Mooibroek, T.J.; Gamez, P.; Reedijk, J. Lone pair– π interactions: A new supramolecular bond? *CrystEngComm* **2008**, *10*, 1501–1515. [[CrossRef](#)]
25. Jakobsche, C.E.; Choudhary, A.; Miller, S.J.; Raines, R.T. $n \rightarrow \pi^*$ Interaction and $n(\pi)$ Pauli Repulsion Are Antagonistic for Protein Stability. *J. Am. Chem. Soc.* **2010**, *132*, 6651–6653. [[CrossRef](#)]
26. Kramer, K.J.; Choudhary, A.; Raines, R.T. Intimate Interactions with Carbonyl Groups: Dipole–Dipole or $n \rightarrow \pi^*$? *J. Org. Chem.* **2013**, *78*, 2099–2103. [[CrossRef](#)]
27. Bartlett, G.J.; Newberry, R.W.; Van Veller, B.; Raines, R.T.; Woolfson, D.N. Interplay of Hydrogen Bonds and $n \rightarrow \pi^*$ Interactions in Proteins. *J. Am. Chem. Soc.* **2013**, *135*, 18682–18688. [[CrossRef](#)]
28. Singh, S.K.; Das, A. The $n \rightarrow \pi^*$ interaction: A rapidly emerging non-covalent interaction. *Phys. Chem. Chem. Phys.* **2015**, *17*, 9596–9612. [[CrossRef](#)]
29. Velásquez, J.D.; Echeverría, J.; Alvarez, S. Effect of the Substituents on the Nature and Strength of Lone-Pair–Carbonyl Interactions in Acyl Halides. *Cryst. Growth Des.* **2019**, *11*, 6511–6518. [[CrossRef](#)]
30. Newberry, R.W.; Raines, R.T. The $n \rightarrow \pi^*$ Interaction. *Acc. Chem. Res.* **2017**, *50*, 1838–1846. [[CrossRef](#)]
31. Doppert, M.T.; van Overeem, H.; Mooibroek, T.J. Intermolecular π -hole/ $n \rightarrow \pi^*$ interactions with carbon monoxide ligands in crystal structures. *Chem. Commun.* **2018**, *54*, 12049–12052. [[CrossRef](#)] [[PubMed](#)]
32. van der Werve Ad, R.; van Dijk, Y.R.; Mooibroek, T.J. π -Hole/ $n \rightarrow \pi^*$ interactions with acetonitrile in crystal structures. *Chem. Commun.* **2018**, *54*, 10742–10745. [[CrossRef](#)] [[PubMed](#)]
33. Zukerman-Schpector, J.; Haiduc, I.; Tiekink, E.R.T. The metal–carbonyl $\cdots\pi$ (aryl) interaction as a supramolecular synthon for the stabilisation of transition metal carbonyl crystal structures. *Chem. Commun.* **2011**, *47*, 12682–12684. [[CrossRef](#)] [[PubMed](#)]
34. Zukerman-Schpector, J.; Haidu, I.; Tiekink, E.R.T. Supramolecular Self-assembly of Transition Metal Carbonyl Molecules Through M–CO(Lone Pair) $\cdots\pi$ (Arene) Interactions. *Adv. Organomet. Chem.* **2012**, *60*, 49–92.
35. Wan, C.-Q.; Chen, X.-D.; Mak, T.C.W. Supramolecular frameworks assembled via intermolecular lone pair–aromatic interaction between carbonyl and pyridyl groups. *CrystEngComm* **2008**, *10*, 475–478. [[CrossRef](#)]
36. Echeverría, J. Intermolecular Carbonyl Carbonyl Interactions in Transition-Metal Complexes. *Inorg. Chem.* **2018**, *57*, 5429–5437. [[CrossRef](#)]
37. Murcia-García, C.; Bauzá, A.; Schnakenburg, G.; Frontera, A.; Streubel, R. Surprising behaviour of M–CO(lone pair) $\cdots\pi$ (arene) interactions in the solid state of fluorinated oxaphosphirane complexes. *CrystEngComm* **2015**, *17*, 1769–1772. [[CrossRef](#)]
38. Mark-Lee, W.F.; Chong, Y.Y.; Kassim, M.B. Supramolecular structures of rhenium (I) complexes mediated by ligand planarity via the interplay of substituents. *Acta Crystallogr. Sect. C Struct. Chem.* **2018**, *74*, 997–1006.
39. Kia, R.; Hosseini, M.; Abdollahi, A.; Mahmoudi, M. Intermolecular C–H \cdots O and $n \rightarrow \pi^*$ and short intramolecular $\sigma \rightarrow \pi^*$ interactions in the molybdenum(0) tetracarbonyl complex of a very twisted 14-membered tetraazaannulene macrocyclic ligand: Structural and computational studies. *CrystEngComm* **2019**, *21*, 5222–5226. [[CrossRef](#)]
40. Kia, R.; Mahmoudi, S.; Raithby, P.R. New rhenium–tricarbonyl complexes bearing halogen-substituted bidentate ligands: Structural, computational and Hirshfeld surfaces studies. *CrystEngComm* **2019**, *21*, 77–93. [[CrossRef](#)]

41. Villegas, J.M.; Stoyanov, S.R.; Huang, W.; Rillema, D.P. A spectroscopic and computational study on the effects of methyl and phenyl substituted phenanthroline ligands on the electronic structure of Re(I) tricarbonyl complexes containing 2,6-dimethylphenylisocyanide. *Dalton Trans.* **2005**, *34*, 1042–1051. [[CrossRef](#)] [[PubMed](#)]
42. Kliegman, J.M.; Barnes, R.K. Glyoxal derivatives-I: Conjugated aliphatic diimines from glyoxal and aliphatic primary amines. *Tetrahedron* **1970**, *26*, 2555–2560. [[CrossRef](#)]
43. Clark, R.C.; Reid, J.S. The analytical calculation of absorption in multifaceted crystals. *Acta Cryst.* **1995**, *A51*, 887–897. [[CrossRef](#)]
44. Dolomanov, O.V.; Bourhis, L.J.; Gildea, R.J.; Howard, J.A.K.; Puschmann, H. OLEX2: A complete structure solution, refinement and analysis program. *J. Appl. Cryst.* **2009**, *42*, 339–341. [[CrossRef](#)]
45. Sheldrick, G.M. A short history of SHELX. *Acta Cryst.* **2008**, *A64*, 112–122. [[CrossRef](#)]
46. Spek, A.L. Structure validation in chemical crystallography. *Acta Cryst.* **2009**, *D65*, 148–155. [[CrossRef](#)]
47. Frisch, M.J.; Trucks, G.W.; Schlegel, H.B.; Scuseria, G.E.; Robb, M.A.; Cheeseman, J.R.; Scalmani, G.; Barone, V.; Mennucci, B. *Gaussian 09, Revision A.02*; ScienceOpen: Berlin, Germany, 2014.
48. Perdew, J.P.; Burke, K.; Ernzerhof, M. Generalized Gradient Approximation Made Simple. *Phys. Rev. Lett.* **1996**, *77*, 3865. [[CrossRef](#)]
49. Andrae, D.; Häußermann, U.; Dolg, M.; Stoll, H.; Preuß, H. Energy-adjusted ab initio pseudopotentials for the second and third row transition elements. *Theor. Chim. Acta* **1990**, *77*, 123–141. [[CrossRef](#)]
50. Cotton, F.A.; Karihanzel, C.S. Vibrational Spectra and Bonding in Metal Carbonyls. I. Infrared Spectra of Phosphine-substituted Group VI Carbonyls in the CO Stretching Region. *J. Am. Chem. Soc.* **1962**, *84*, 4432–4438. [[CrossRef](#)]
51. Klein, A.; Vogler, C.; Kaim, W. The δ in $18 + \delta$ Electron Complexes: Importance of the Metal/Ligand Interface for the Substitutional Reactivity of “Re(0)” Complexes (α -diimine)Re^I(CO)₃(X). *Organometallics* **1996**, *15*, 236–244. [[CrossRef](#)]
52. Staal, L.H.; Oskam, A.; Vrieze, K. The syntheses and coordination properties of M(CO)₃X(DAB) (M = Mn, Re; X = Cl, Br, I; DAB = 1,4-diazabutadiene). *J. Organomet. Chem.* **1979**, *170*, 235–245. [[CrossRef](#)]
53. Vollmer, M.V.; Machan, C.W.; Clark, M.L.; Antholine, W.E.; Agarwal, J.; Schaefer III, H.F.; Kubiak, C.P.; Walensky, J.R. Synthesis, Spectroscopy, and Electrochemistry of (α -Diimine)M(CO)₃Br, M = Mn, Re, Complexes: Ligands Isoelectronic to Bipyridyl Show Differences in CO₂ Reduction. *Organometallics* **2015**, *34*, 3–12. [[CrossRef](#)] [[PubMed](#)]
54. Abramov, P.A.; Dmitriev, A.A.; Kholin, K.V.; Gritsan, N.P.; Kadirov, M.K.; Gushchin, A.L.; Sokolov, M.N. Mechanistic study of the [(dpp-bian)Re(CO)₃Br] electrochemical reduction using in situ EPR spectroscopy and computational chemistry. *Electrochim. Acta* **2018**, *270*, 526–534. [[CrossRef](#)]
55. Johnson, E.R.; Keinan, S.; Mori-Sánchez, P.; Contreras-García, J.; Cohen, A.J.; Yang, W. Revealing Noncovalent Interactions. *J. Am. Chem. Soc.* **2010**, *132*, 6498–6506. [[CrossRef](#)]
56. Contreras-García, J.; Johnson, E.R.; Keinan, S.; Chaudret, R.; Piquemal, J.-P.; Beratan, D.N.; Yang, W. NCIPLOT: A program for plotting non-covalent interaction regions. *J. Chem. Theory Comput.* **2010**, *7*, 625–632. [[CrossRef](#)]
57. Usoltsev, A.N.; Adonin, S.A.; Novikov, A.S.; Samsonenko, D.G.; Sokolova, M.N.; Fedin, V.P. One-dimensional polymeric polybromotellurates (IV): Structural and theoretical insights into halogen···halogen contacts. *CrystEngComm* **2017**, *19*, 5934–5939. [[CrossRef](#)]
58. Glendening, E.D.; Landis, C.R.; Weinhold, F. Natural bond orbital methods. *WIREs Comput. Mol. Sci.* **2012**, *2*, 1–42. [[CrossRef](#)]

